

# Wave propagation and shock formation in different magnetic structures

R. Centeno<sup>1,2</sup>, M. Collados<sup>2</sup>, J. Trujillo Bueno<sup>2,3</sup>

rce@ucar.edu, mcv@iac.es, jtb@iac.es

## ABSTRACT

Velocity oscillations "measured" simultaneously at the photosphere and the chromosphere -from time series of spectropolarimetric data in the 10830 Å region- of different solar magnetic features allow us to study the properties of wave propagation as a function of the magnetic flux of the structure (i.e. two different-sized sunspots, a tiny pore and a facular region). While photospheric oscillations have similar characteristics everywhere, oscillations measured at chromospheric heights show different amplitudes, frequencies and stages of shock development depending on the observed magnetic feature. The analysis of the power and the phase spectra, together with simple theoretical modeling, lead to a series of results concerning wave propagation within the range of heights of this study. We find that, while the atmospheric cut-off frequency and the propagation properties of the different oscillating modes depend on the magnetic feature, in all the cases the power that reaches the high chromosphere above the atmospheric cut-off comes directly from the photosphere by means of linear vertical wave propagation rather than from non-linear interaction of modes.

*Subject headings:* Sun : photosphere, Sun : chromosphere, Sun : magnetic fields, techniques : polarimetric, shock waves

## 1. Introduction

Encrypted in the oscillatory behavior of the solar atmosphere lies crucial information for understanding its dynamical and physical properties. The stratification caused by gravity,

---

<sup>1</sup>High Altitude Observatory (NCAR) The National Center for Atmospheric Research is sponsored by the National Science Foundation, Boulder CO 80301, USA

<sup>2</sup>Instituto de Astrofísica de Canarias, 38205, La Laguna, Tenerife (Spain)

<sup>3</sup>Consejo Superior de Investigaciones Científicas (Spain)

together with the presence of magnetic fields, leads to a variety of magneto-gravity-acoustic modes (Khomenko & Collados 2006; Abdelatif & Thomas 1987; Thomas 1983). By analyzing the local properties of oscillations and wave propagation we can infer information about the stratification and dynamics of different atmospheric structures.

Wave propagation is an efficient means of carrying energy between different layers of the atmosphere and of dissipating it efficiently through the formation and breaking of shocks (Mihalas & Wiebel-Mihalas 1984). Although acoustic (slow-mode) heating is not important for the upper atmosphere (Athay & White, 1979; White & Athay, 1979), the role that wave propagation plays in the heating problem is still one of the most challenging open debates amongst solar physics researchers.

The first measurements of oscillations in the quiet Sun (Leighton et al. 1962) came nearly a decade before the first detection of sunspot oscillations were reported (Beckers & Tallant 1969). Since then, many works have tried to put the pieces of the puzzle together (see Lites 1992; Bogdan & Judge 2006, for a comprehensive review of the literature of wave propagation in sunspots).

Oscillations above sunspots show a 5-minute periodicity in the photosphere. However, at chromospheric levels and higher up, this picture changes into a 3-minute saw-tooth pattern (see e.g. Lites 1986; Lites 1986b; Socas-Navarro Trujillo Bueno and Ruiz Cobo 2000; Collados et al. 2001; Brynildsen et al. 2003; Brynildsen et al. 2004). Several hypotheses have attempted to explain the origin of the chromospheric 3-min oscillations. Zhugzhda, Locans & Staude (1985) proposed a model with a resonant chromospheric cavity that would explain the presence of multiple peaks in the chromospheric power spectrum together with the 3 minute period. On the other hand, Gurman & Leichbacher (1984) suggested an origin based on the non-linear interaction of photospheric modes. Centeno, Collados and Trujillo Bueno (2006a) showed that the chromospheric 3-minute signal in the umbrae of sunspots is a result of linear wave propagation of the photospheric perturbations in the 6 mHz range, thus ruling out the non-linear origin for these oscillations.

Observations above facular and network areas report 5-minute oscillations at chromospheric heights (see e.g. Krijger et al. 2001; Lites et al. 1993; De Pontieu et al. 2003a; Centeno et al. 2006b) and higher up. For this to happen, the atmospheric cut-off frequency must be reduced, allowing the "evanescent" photospheric 5-minute oscillations propagate into the chromosphere. De Pontieu et al. (2003, 2004) suggested that the inclination of magnetic fields plays an important role in this p-mode leakage with enough energy to give rise to the dynamic jets that are observed in active region fibrils. With this idea in mind, Jefferies et al. (2006) suggested that inclined flux tubes might explain the observed properties of waves at chromospheric heights.

The effective cut-off frequency is lowered by the cosine of the inclination angle with respect to the local vertical. Thus, if the magnetic field is sufficiently inclined, the flux tubes will channel the photospheric 5-minute perturbations all the way up into the chromosphere and corona. An alternate possibility takes into account a departure from adiabaticity due to radiative losses, which results in a reduced cut-off frequency (Roberts 2006; Centeno et al. 2006b; Khomenko et al. 2008) that allows the 5-minute modes to propagate.

Simultaneous time-series observations of various spectral lines that sample different regions of the solar atmosphere is one of the most useful techniques for studying wave propagation. For the analysis that follows we measure simultaneously the full Stokes vector of the photospheric Si I 10827 Å line and of the chromospheric He I 10830 Å multiplet on different magnetic targets. The analysis of the photospheric and chromospheric LOS velocity oscillations and the relation between them give us information about the behavior of the atmosphere: the propagation of photospheric disturbances, the amplification of the oscillations as they travel towards higher layers of the atmosphere, the cut-off frequency below which the oscillation modes do not propagate, the development of shocks and so on. We carry out a comparative study among 4 magnetic structures with different magnetic fluxes: a rather big sunspot (analyzed in Centeno et al. 2006a, hereafter Paper I), a smaller one, a pore that has developed no penumbra and a facular region. The physical properties of the atmosphere in each case determines how the propagation of the photospheric perturbations takes place and viceversa.

The outline of the paper is as follows: after a brief description of the observations and the inversion procedures in Section 2, Section 3 continues to describe the properties of the oscillations measured at photospheric and chromospheric heights. Section 4 analyzes the relations between them, which are determined by the propagation properties of the atmosphere in each case. The comparison with a simple model of linear vertical wave propagation in a magnetized atmosphere with radiative losses will yield to a qualitative understanding of the origin of the chromospheric oscillations in the analyzed magnetic structures. A brief discussion of the results is presented in Section 5.

## 2. Observations

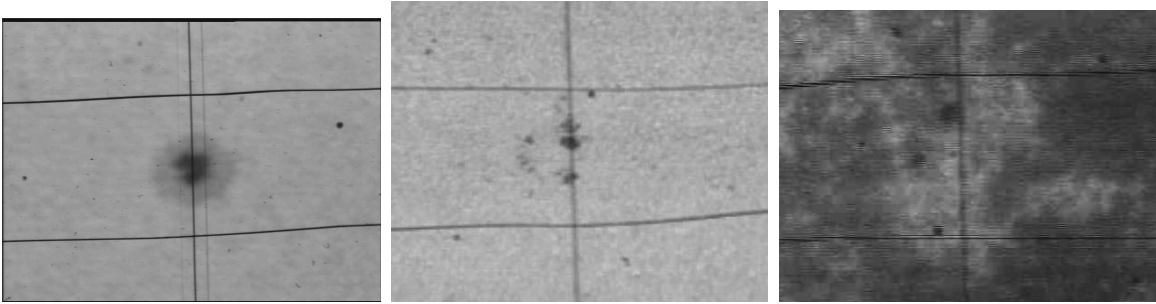


Fig. 1.— White light slitjaw images for the small sunspot and the pore, and Ca K image for the facular region. In all the cases, the vertical line corresponds to the shadow of the spectrograph slit (which was kept fixed during each run) and horizontal lines delimit the field of view of the polarimeter ( $\sim 40''$ ). Of the three pores showed in the second image, we chose the central one to carry out the analysis presented in this paper.

The observations were carried out at the German Vacuum Tower Telescope (VTT) of the Observatorio del Teide between September 2000 and June 2002, using the Tenerife Infrared Polarimeter (TIP, Martínez Pillet et al. 1999). This instrument allowed us to measure simultaneously the four Stokes profiles for all the spatial positions along the spectrograph slit at each scanning step. The slit ( $0''.5$  wide and  $40''$  long) was placed over the targets and was kept fixed during the entire observing run (approx. 1 hour for each target). The image stability throughout the time series was achieved by using a correlation tracker device (Schmidt & Kentischer 1995; Ballesteros et al. 1996) which compensated, to first order, for the solar rotation as well as for the image motion induced by the Earth’s high frequency atmospheric variability, thus minimizing the image jitter. Despite of being observed at very different moments, the quality is similar throughout the four datasets, and the instrument components and configuration were identical in all cases. The spatial resolution varies roughly between  $1''$  and  $1''.5$  (the worst data-set being the one that corresponds to the small sunspot). Details on the 4 data-sets analyzed in this paper are given in Table 2. Fig. 1 shows the slit-jaw images for the small sunspot, the pore and the facula. The size of the structure refers to the umbra in the case of the sunspots and to the enhanced bright region as seen in the Ca K slit-jaw in the case of the facula. The data-set corresponding to the big sunspot was one of those used throughout Paper I. We chose the more regular and homogeneous of the two sunspots and we only included it here for a sake of completeness, to compare it with the results from the other 3 magnetic structures.

Flat-field and dark current measurements were performed at the beginning and the end of all observing runs, and, in order to compensate for the telescope instrumental polarization, we also took a series of polarimetric calibration images. The calibration optics (see Collados 1999) allows us to obtain the Mueller matrix of the light path between the instrumental calibration subsystem and the polarimeter. This process leaves a section of the telescope without being calibrated, so further corrections of the residual cross-talk among Stokes parameters were done: the I to Q, U, and V cross-talk were removed by forcing the continuum polarization to zero, and the circular and linear polarization mutual cross-talks were estimated by means of statistical techniques (Collados 2003).

	big sunspot	small sunspot	pore	facular region
Date	May 9, 2001	Sep 30, 2000	Jun 13, 2002	Jun 14, 2002
Pos X ["]	-392	557	-339	-90
Pos Y ["]	-163	102	306	-291
$\mu = \cos\theta$	0.89	0.81	0.88	0.94
Duration [s]	4214	3922	4842	4873
Cadence [s]	2.1	7.9	5.4	5.4
Noise	$2 \cdot 10^{-3}$	$7 \cdot 10^{-3}$	$2 \cdot 10^{-3}$	$10^{-3}$
Size ["]	16	10	4	30

Table 1: Details of the four data-sets obtained with TIP. Positions X and Y represent terrestrial E-W and N-S directions and are measured from sun center.

The observed spectral range spanned from 10825 to 10833 Å, with a spectral sampling of 31 mÅ per pixel. This spectral region is a powerful diagnostic window for the solar atmospheric properties since it contains valuable information coming from two different layers in the atmosphere. It includes a photospheric Si I line at 10827 Å and a chromospheric He I triplet centered around 10830 Å. The Si line is formed in the high photosphere. The response function (Ruiz Cobo & del Toro Iniesta, 1994) of the intensity profile to the temperature shows a height of formation between 300 and 540 km above the base of the photosphere (Bard and Carlsson, 2008). The He multiplet is formed in the high chromosphere (Avrett et al. 1994; Schmidt et al. 1994; Sánchez-Andrade Nuño et al. 2007; Centeno et al. 2008), although the exact location depends critically on the atmospheric stratification and the coronal illumination coming from above, that triggers the formation of the multiplet. Thus, the difference in height between the photospheric and the chromospheric indicators ranges between 1000 and 1500 km. The He triplet serves as a unique diagnostic tool for chromospheric magnetic fields (see Lagg 2007, for a recent review).

In order to infer the physical parameters of the magnetized atmosphere in which the measured spectral lines were generated, we carried out the full Stokes inversion of both the silicon line and the helium triplet for the whole time series of observations and for all four data-sets. The Si line was treated in Local Thermodynamic Equilibrium (LTE) and inverted with the code LILIA (Socas-Navarro 2001). This inversion code yields the line-of-sight (LOS) velocity, magnetic field, temperature, density and electron pressure stratification of the atmosphere in the layers where the spectral line radiation is generated. The observations of the He I triplet were interpreted with our Milne-Eddington inversion code of Stokes profiles induced by the Zeeman effect, which is a suitable strategy for extracting information on the LOS velocity and gives a reliable estimation of the field strength from the full Stokes vector (see Trujillo Bueno & Asensio Ramos 2007; Centeno et al, in press). We did not consider the incomplete Paschen-Back effect in the modeling, so the magnetic field strength is underestimated by up to a 20% (Sasso et al. 2005). However, in the analysis carried out in this paper we focus on the velocities, which are not affected by this. By inverting the whole time series we were able to obtain the temporal variability of several physical quantities (line-of-sight velocity, magnetic field intensity and orientation, ...) at the photosphere and chromosphere of the four magnetic structures. Both inversion codes took into account only one atmospheric component (one velocity and one magnetic field value). Only in the case of the facula, a stray light component was included to account for the non-magnetic part of the spectral profiles.

The magnetic field values yielded by the inversions are given in the line-of-sight (LOS) reference system (which depends on the position of the target on the solar disk). The azimuth origin, defined by the polarimetric calibration optics of the telescope, is referenced to the

Earth’s North-South direction. In order to determine how vertical the inferred magnetic fields are, we have to transform them to the local vertical reference frame. The  $180^\circ$  ambiguity in the azimuth leads to two possible inclination values in the new reference system. The flotability of strong magnetic flux tubes can be used as a physical argument to choose the more vertical solution over the other option. The photospheric magnetic fields obtained from the inversion of the Si line turn out to be very vertical (with a range of inclinations between  $0^\circ$  and  $20^\circ$ ) in all the cases. The He lines show barely any linear polarization at all due to the weaker magnetic field regime in the high chromosphere.

Throughout the rest of this paper we will focus on the results concerning the LOS velocity oscillations, which are the line-of-sight projection of the plasma movements along the magnetic field lines. All the targets are relatively close to disk center (the farther one having a heliocentric angle of  $\mu = \cos\theta = 0.81$ ), so this means that the maximum projection effect would happen for the small sunspot, for which the LOS forms an angle of  $\sim 35^\circ$  with the local vertical. Taking into account the estimated height difference between the formation of the photospheric and the chromospheric indicators ( $\sim 1000 - 1500$  km), this angle would lead to a maximum projected horizontal displacement (for two positions on the same vertical) of some 900 km. The spatial resolution in our data was limited by seeing, which we estimated to be of the order of  $\sim 1 - 1.5''$ , so the displacement due to projection effects will be barely noticeable in the worst case.

### 3. Oscillations and Shock Waves

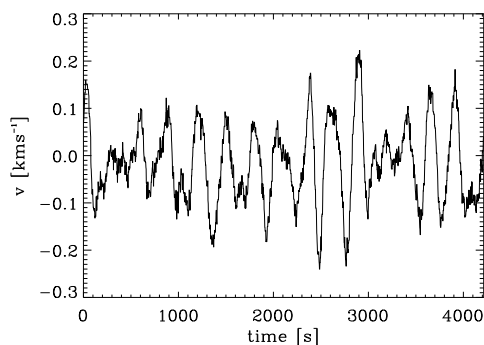


Fig. 2.— Photospheric oscillations for one position inside the umbra of sunspot #1. The rest of the structures analyzed in this work show a qualitatively similar behavior at photospheric levels.

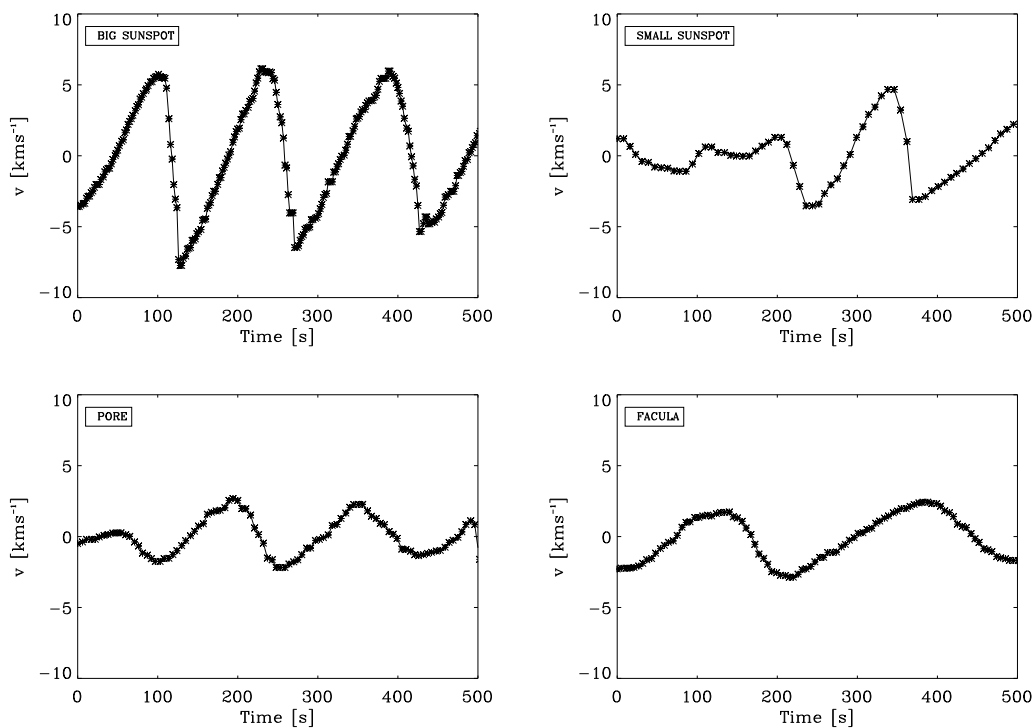


Fig. 3.— Chromospheric oscillations in different magnetic features as seen by the He I 10830 Å triplet. From left to right and top to bottom, the panels depict a typical velocity profile for one position inside the umbra of a big sunspot, the umbra of small sunspot, a pore and a facula. In all the cases, asterisks represent the measured values, equispaced in time.

Photospheric velocity<sup>1</sup> oscillations (see Fig. 2), retrieved from the inversion of the Si I line, show the same characteristics everywhere: a typical 5-min period, 300–400 m s<sup>-1</sup> peak to peak amplitudes and fairly sinusoidal patterns.

On the other hand, chromospheric velocity oscillations (encoded in the Doppler shift of the He I triplet) show very different behavior depending on the magnetic structure. Fig. 3 depicts a detail of the chromospheric oscillation pattern in the four regions analyzed. From left to right and top to bottom, the panels show the velocity variations in the umbrae of the big and medium-sized sunspots, the pore and the facular region. The asterisks represent the measured values, equispaced in time. The departure from a sinusoidal behavior is a signature of the passage of shock waves through this layer of the atmosphere. It is clear from Fig. 3 that, as the magnetic flux of the structure decreases, the amplitude of the oscillations also becomes smaller (from  $\sim 15$  km s<sup>-1</sup> in the big sunspot to  $\sim 3$ –4 km s<sup>-1</sup> in the facula). Note that the projection effects are larger for the three sunspot-like features than for the facula because they are farther away from disk center. Assuming that the plasma movements are directed along the field lines - parallel to the local vertical- then the actual oscillation amplitudes for the sunspots are even larger than the values given above. The steepness and the frequency of appearance of the shocks is also correlated with the magnetic flux of the observed feature.

The chromospheric oscillations in the facular region present a particularity that is not shared by the sunspot-like structures (i.e. both sunspots and the pore). While the latter show a characteristic 3-minute pattern, the facular region presents, in contrast, an obvious 5-minute period at chromospheric heights.

---

<sup>1</sup>The sign convention used throughout this paper is such that negative velocities correspond to material approaching the observer along the line-of-sight.

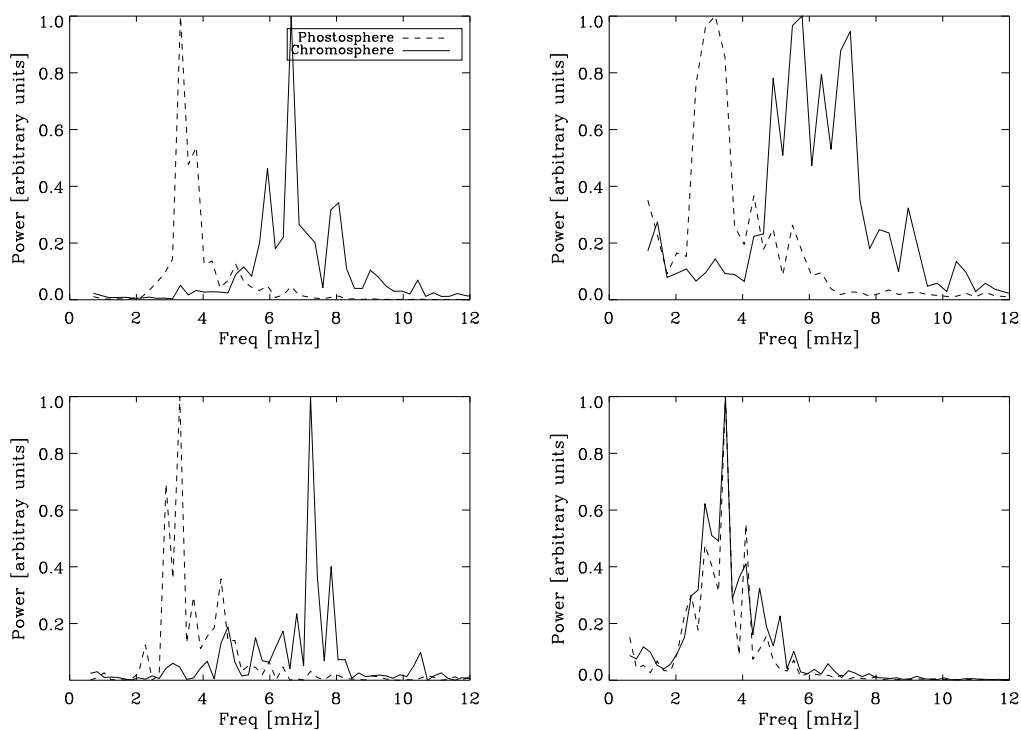


Fig. 4.— Normalized LOS velocity power spectra of the four analyzed regions. From left to right and top to bottom, the panels show the photospheric (dashed) and chromospheric (solid) power spectra, (averaged over the length that the structure spanned along the spectrograph slit and normalized to their maximum), for the big sunspot, the small sunspot, the pore and the facular region.

Fig. 4 illustrates the difference between the spectral composition of the oscillation patterns of the sunspot-like structures and the facular region. From left to right and top to bottom, the panels represent the average photospheric (*dashed*) and chromospheric (*solid*) power spectra in the four magnetic features. While in the sunspot-like structures the majority of the oscillatory energy is concentrated around different frequency regimes in the photosphere and the chromosphere, the facular power spectra show a strikingly similar behavior at both heights (with the maximum power lying at 3.3 mHz and the secondary peaks being co-located and showing pretty much the same distribution).

One could attribute this to the helium triplet being formed lower in the atmosphere (closer to the region of formation of the Silicon line). However, this can be ruled out for two reasons: 1) the oscillations derived from the He lines have at least ten times the amplitude of those measured with the Si line, indicating that they are clearly chromospheric. 2) if the He triplet is formed by the triggering effect of the coronal irradiance (see Avrett et al. 1994; Centeno et al. 2008), there is no way the lines can have a contribution function from the photosphere, but it can only come from the high chromosphere.

The 5-minute chromospheric oscillations appear as a consequence of the reduced cut-off frequency in facular regions.

#### 4. Wave propagation

For the wave propagation analysis we will follow the strategy adopted in Paper I. First, we will analyze the information given by the mean power, phase difference and amplification spectra. This will allow us to identify the propagation regime of the wave modes in each case and determine the cutoff frequency and the amplification of the oscillations as the waves travel through the atmosphere. Then, we will try to reproduce these observables with a simple model of vertical linear wave propagation along constant magnetic field lines in a stratified atmosphere. The theoretical modeling will allow us to make a prediction about the time delay between the signals measured at the photosphere and the chromosphere, which will be contrasted with what is obtained by mere cross-correlation of the measured velocity maps at both heights.

##### 4.1. Phase difference and cutoff frequencies

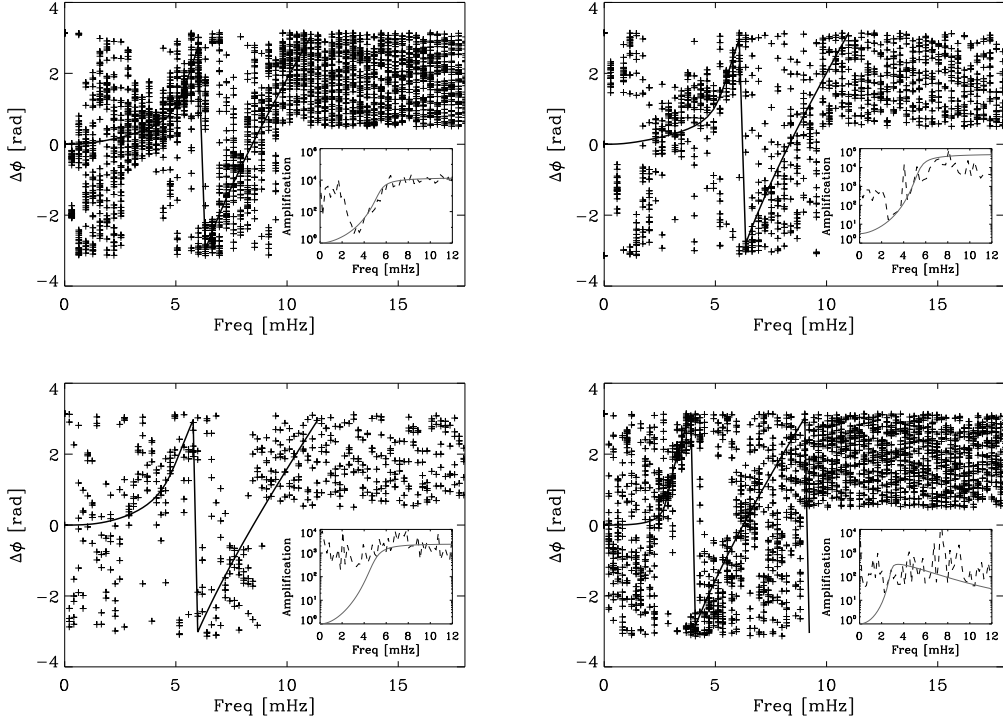


Fig. 5.— Phase difference between photospheric and chromospheric oscillations as a function of frequency for the four magnetic structures (from left to right and top to bottom the panels correspond to the umbrae of the big and small sunspots, the pore and the facula). Each cross on the figure was computed as the difference between the phase of the chromospheric and the photospheric oscillation for a unique position along the slit and a particular frequency. The small insets show the respective amplification spectra. Solid lines correspond to the best fit to a model of linear wave propagation in a stratified isothermal atmosphere with radiative losses, permeated by a constant vertical magnetic field.

Fig. 5 shows the phase difference between the photospheric and the chromospheric oscillations for the four magnetic features analyzed in this paper. Each cross on the panels was computed as the difference between the phase of the chromospheric and the photospheric oscillations for one position along the slit and one frequency value. The turn-off points in the phase spectra correspond to the effective cut-off frequencies of the atmosphere. Oscillations with lower frequencies will not be able to make it through the atmosphere and, thus, will remain trapped producing stationary waves. Above the cut-off value, perturbations propagate upwards freely into the chromosphere. Note that in the case of the sunspot-like structures the atmospheric cut-off stands around 4 mHz, inhibiting the propagation of lower frequency modes. This has strong implications on what happens to the photospheric oscillatory energy -which lies below the cut-off value- and strikes the question of the origin of the 3-minute chromospheric power in such structures. Paper I addressed this question and proved that, inside the umbrae of sunspots, the chromospheric 3-minute oscillations come from the upward linear propagation of the photospheric 3-minute power rather than from the non-linear interaction and redistribution of the energy stored in the 5-minute photospheric modes. This means that, while the 5-minute photospheric component stays trapped in the atmosphere giving rise to stationary waves, the 3-minute photospheric component travels upward through the atmosphere driving the chromospheric oscillations.

The case of the facular region is somewhat different. Now, the cut-off frequency is lower than that of the typical photospheric modes, thus allowing them to propagate through the atmosphere. This would explain why the facular chromospheric power spectrum peaks around 3.3 mHz, since all the 5-minute photospheric power can travel freely upward into the high chromosphere.

The small inset in the lower right corner of each panel of Fig. 5 represents the corresponding amplification spectrum (dashed line), this is, the ratio of the chromospheric power over the photospheric power as a function of frequency. For decreasing magnetic flux, the amplification of the power in the propagation regime (i.e. above the cut-off frequency) also decreases.

## 4.2. Model

A simple model of upward linear wave propagation in an isothermal stratified atmosphere permeated by a constant vertical magnetic field (described in Paper I, but originally accounted for by Souffrin in 1972) was chosen to further explain the observations. Energy exchange by radiative losses is permitted by Newton’s cooling law, which accounts for the damping of the temperature fluctuations with a typical relaxation time  $\tau_R$  (Spiegel 1957;

Kneer & Trujillo Bueno 1987):

$$\tau_R = \frac{\rho c_v}{16\chi\sigma_R T^3} \quad (1)$$

where  $\chi$  is the grey absorption coefficient and  $\sigma_R$  the Stefan-Boltzmann constant. The solution  $A(z) = D e^{z/2H_0} e^{ik_z z} e^{i\omega t}$  substituted into the wave equation:

$$\hat{c}^2 \frac{d^2 A(z)}{dz^2} - \hat{\gamma} g \frac{dA(z)}{dz} + \hat{\omega}^2 A(z) = 0 \quad (2)$$

yields a dispersion relation:

$$k_z^2 = \frac{\omega^2 - \hat{\omega}_{ac}^2}{\hat{c}^2}, \quad (3)$$

where  $k_z$  is the vertical wave number,  $H_0$  the pressure scale height, and  $\hat{\omega}$  and  $\hat{c}$  were defined in (Bunte & Bogdan 1994):

$$\hat{\omega}_{ac} = \hat{c}/2H_0, \quad \hat{c}^2 = \hat{\gamma} g H_0, \quad \hat{\gamma} = \frac{1 - \gamma i\omega\tau_R}{1 - i\omega\tau_R} \quad (4)$$

This results in a 3-free-parameter model, with the temperature,  $T$ , the vertical distance between the measured oscillations,  $\Delta z$ , and the typical radiative cooling time,  $\tau_R$ , as the fitting coefficients. For a more detailed description, we refer the reader to Paper I, Bunte and Bogdan (1994), Mihalas & Wiebel-Mihalas (1984) and Souffrin (1972).

The model assumes a magnetic field that is aligned with gravity. The full Stokes inversion of the photospheric Si line in our data-sets shows that, in all cases, the deviation of the magnetic field direction from the local vertical never exceeds  $20^\circ$ , being close to  $0^\circ$  for most of the pixels (within the uncertainties).

The solid lines (both in the bigger panels and in the insets) of Fig. 5 correspond to the best fit of the model to the data. There, all the pixels of the observed targets are plotted together. The free parameters of the model were adjusted to explain, simultaneously, the average observed phase difference and average amplification spectrum. The fit has to account for the turn-off point due to the cut-off frequency and the steepness of the phase spectrum together with the magnitude of the amplification of the power. The different parameters have very distinct effects on the resulting curves. For instance, while the radiative cooling time controls the position of the turn-off point, the height difference determines the magnitude

of the amplification of the signals from the photosphere to the chromosphere. Table 4.2 compiles the values of the resulting fitting parameters.

	big sunspot	small sunspot	pore	facular region
$T$ [K]	4000	4500	5000	9000
$\Delta z$ [km]	1000	1000	1000	1500
$\tau_R$ [s]	55	30	25	10

Table 2: Fitting parameters used in linear wave propagation modeling

In the sunspot-like structures, as the magnetic flux decreases, the typical cooling time also decreases while the temperature grows. Although quantitatively these numbers are difficult to justify due to the simplicity of the model, they do make sense in a qualitative way. It is no doubt expected that the smaller the structure, the larger the temperature inside it, since its magnetic field becomes more and more incapable of inhibiting the convection process underneath the photosphere. On the other hand, the radiative cooling time is related to the inhomogeneity, taking smaller values the less homogeneous the structure (see Spiegel 1957; Kneer & Trujillo Bueno 1987). The difference in heights remains essentially the same for the three sunspots, while it turns out to be larger in the case of the facula. Sunspot-like features are evacuated structures (due to the balance between magnetic and gas pressure), allowing the coronal EUV irradiance to travel further down into the chromosphere and trigger the formation of the He I 10830 Å triplet at lower layers (see Centeno et al. 2008).

### **4.3. Theoretical prediction and measured time delays**

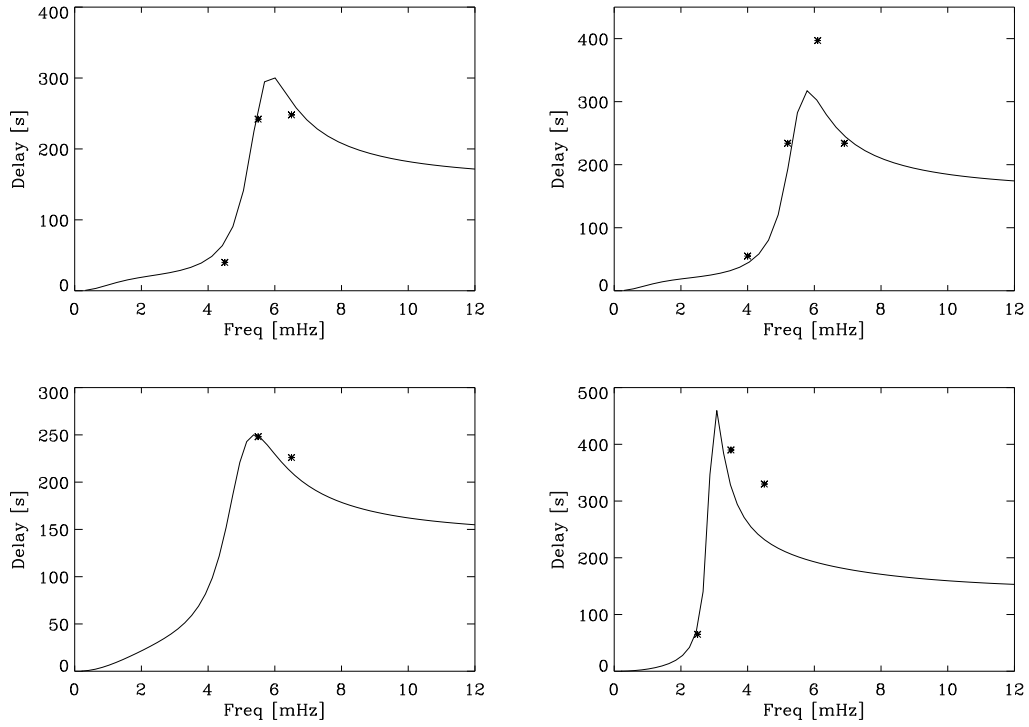


Fig. 6.— Expected and measured time delays. From left to right and top to bottom, the panels correspond to the umbra of the big sunspot (extracted from Paper I), the umbra of the small sunspot, the pore and the facular region. The solid line shows the expected time delay, as a function of frequency, predicted by the model. The asterisks correspond to the measured delays.

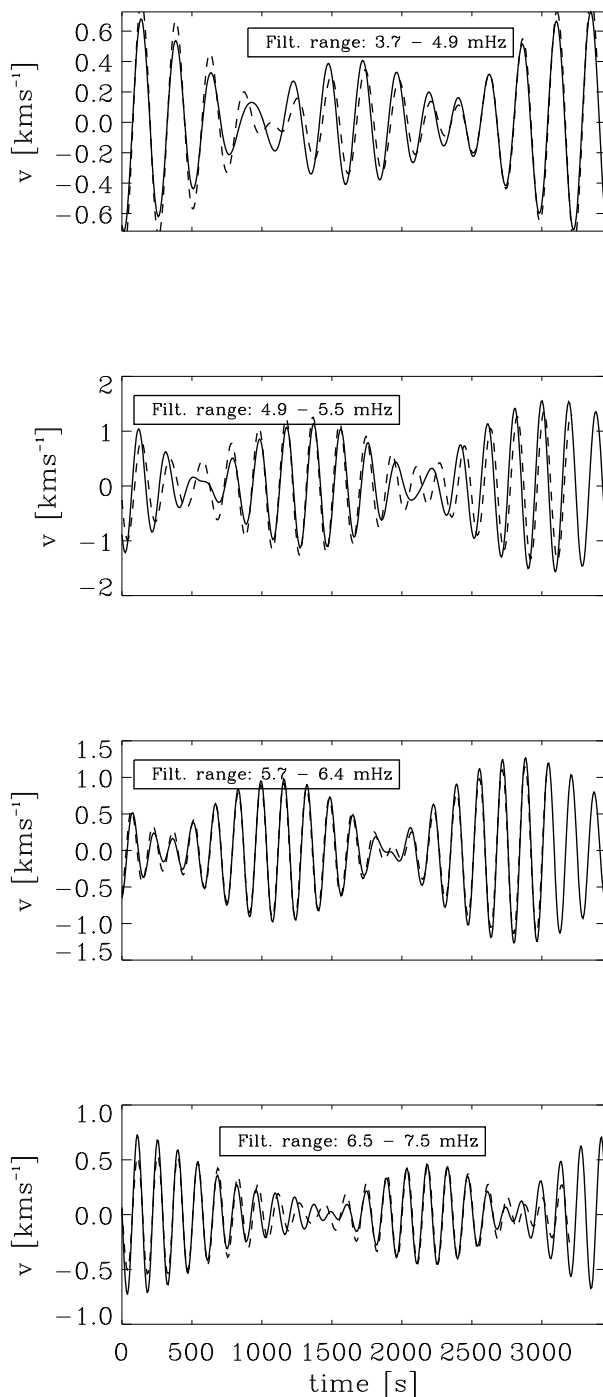


Fig. 7.— Time delays in the umbra of the small sunspot. The panels show the velocities, for one pixel position inside the umbra, filtered in 1 mHz frequency bands around 4, 5, 6 and 7 mHz. Overplotted to the chromospheric velocity (dashed lines) is the photospheric signal (solid lines), filtered in the same frequency band, but amplified and delayed to make it match the latter one. Similar plots for other pixels along the slit result in delays and amplifications that are consistent with those shown here.

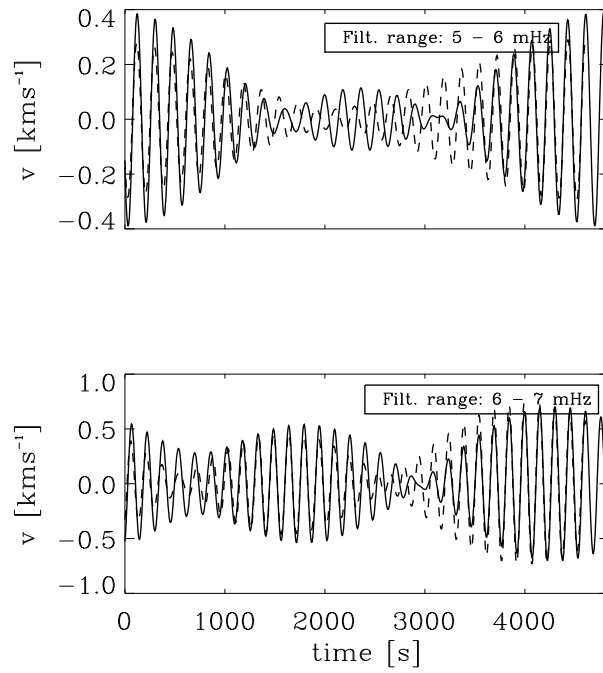


Fig. 8.— Measured time delays inside the pore. Analogous to Fig. 7 except for the filtering bands. From top to bottom, the velocity signals have been filtered in 1 mHz bands around 5.5 and 6.5 mHz, respectively. The photospheric signal was shifted in time and amplified in order to match the chromospheric one.

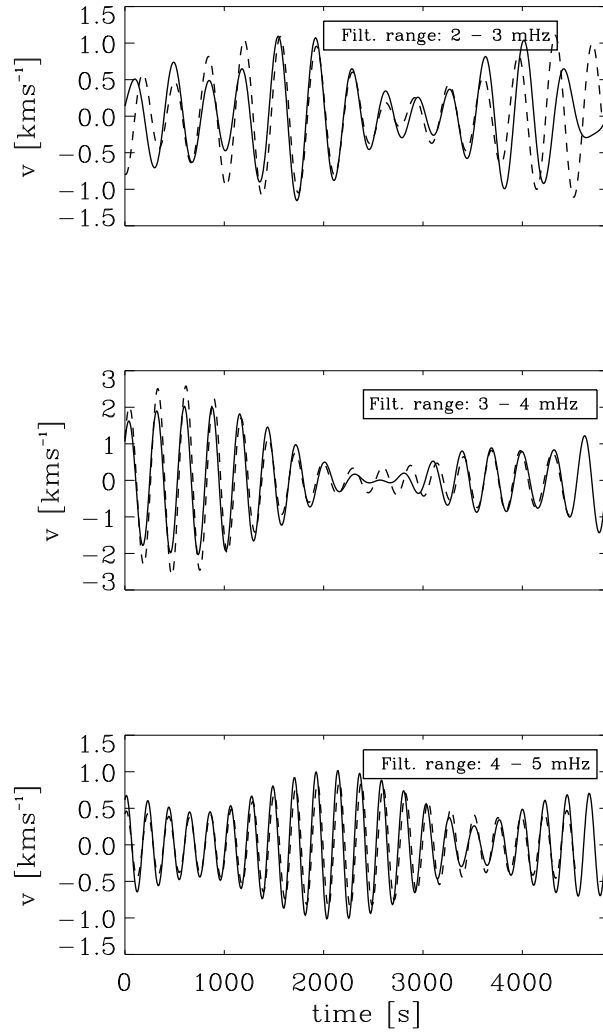


Fig. 9.— Measured time delays inside the facular region. Analogous to Fig. 7 except for the filtering bands. From top to bottom, the velocity signals have been filtered in 1 mHz bands around 2.5, 3.5 and 4.5 mHz, respectively. The photospheric signal was shifted in time and amplified in order to match the chromospheric one.

The solid lines in Fig. 6 show the expected time delays (in the four magnetic structures), as a function of frequency, between the oscillations measured at the photosphere and the chromosphere as derived from the theoretical model. The time delay,  $\Delta t$ , depends on the difference in heights,  $\Delta z$  and the group velocity of the wave packet,  $v_g$ :

$$\Delta t = \frac{\Delta z}{v_g} \quad (5)$$

where

$$v_g = \frac{d\omega}{dk_z} \quad (6)$$

Using the best fitting values for  $\Delta z$ ,  $T$  and  $\tau_R$ , we computed the theoretical time delay from the wave propagation model described above.

If propagation is mainly linear within the 2 - 7 mHz band (as suggested by the good fits of the model to the data) and it takes place along the magnetic field lines, then we should expect to see a correlation of the photospheric and chromospheric oscillation patterns above the cutoff-frequency. It should be possible to determine the time delay from the observations by simply comparing these modulation patterns at both heights. The time shift that yields the maximum correlation will correspond to the measured delay.

However, the theoretical time delays depicted in Fig. 6 show a very strong dependence on the frequency of the oscillating mode, so we have to take this fact into account when doing the comparison. Following the approach taken in Paper I, we first filter both the photospheric and the chromospheric velocity maps in narrow frequency ranges (narrow enough that the expected time delay does not vary significantly within the bandwidth). Then, we compare the photospheric and chromospheric filtered signals finding that we have to apply a certain time shift between them in order to make their external modulation schemes match. This shift corresponds to the time that a perturbation (within the filtering frequency range) originated in at photospheric levels takes to reach the chromosphere.

In the case of the sunspot-like structures, we filtered the velocity maps in several one-mHz bands close to 6 mHz (where the main contribution to the chromospheric power lies). We then compared each pair of filtered maps finding a time shift between them that depended on the frequency range in which the maps were filtered. The four panels of Fig. 7 show the photospheric (solid) and chromospheric (dashed) velocities, for one position inside the umbra of the small sunspot, filtered in  $\sim 1$  mHz frequency bands around 4, 5, 6 and 7 mHz. In each case, the photospheric signal has been amplified and delayed to make it match the

chromospheric one.

This procedure was repeated for several pixels in the umbra. There are coherent patches of a few arcseconds along the slit in which the velocity signals are very similar, so we chose 3 or 4 positions far apart, and measured the delay for each of them finding consistent time shifts and amplification values at the different spatial locations. The uncertainty for the time delay is of the order of 1 - 2 time steps ( $\sim 10 - 15$ s). The measured delays extracted from this method are represented by the asterisks over plotted to the top left panel of Fig. 6. Analogous analyses were carried out for the pore (shown in Fig. 8) and for the big sunspot (in Paper I).

The pore is only 4 arcsecs wide and oscillations are quite coherent throughout the whole structure. Also, there is not a strong modulation of the velocity oscillation pattern, so, in certain frequency bands, it is not clear what time shift gives the larger correlation between photosphere and chromosphere. This is why we only show the results for two frequency bands in Fig. 8.

In the case of the facular region we filtered the velocity maps in three ranges around 3 mHz (where both photospheric and chromospheric power spectra have their main contributions). The remaining analysis is parallel to the former case. The three panels of Fig. 9 show the chromospheric (*solid*) and photospheric (*dashed*) velocity signals filtered around 2.5, 3.5 and 4.5 mHz, respectively. Again, the photospheric signal has been amplified and shifted in time to make it match the chromospheric one.

In all the cases, the amplification factors turn out to be consistent with the values of the amplification spectrum in Fig. 5, and the measured time delays (represented by asterisks superposed to the theoretical time delays in Fig. 6) obtained from the shifts are consistent with the expected values obtained from the model. Even though the theoretical curves predict a very strong variation of the time delay within the 1 mHz filtering bands, the measured delays agree surprisingly well with what is expected by the model.

## 5. Discussion and conclusions

In this paper we have investigated the wave propagation in the atmospheres of four solar magnetic structures with decreasing flux (two different-sized sunspots, a pore and a facular region). Simultaneous and co-spatial measurements of the LOS velocity at the photosphere and the chromosphere of these structures allow us to infer information about the properties of wave propagation from one atmospheric layer to another. A simple model of linear vertical wave propagation in a magnetized stratified medium with radiative losses is enough to explain

the observed phase difference and amplification spectra and the measured time delays.

The inversion of the full Stokes vector in the four structures reveals vertical (i.e. radial) magnetic fields in all cases. The comparison of the photospheric and chromospheric velocity maps, filtered in narrow frequency ranges, shows a pixel to pixel correlation along the slit of the external modulation of the wave pattern (after accounting for a global time shift and a global amplification of the photospheric signal). These two facts are enough to justify the election of a model of linear wave propagation along vertical magnetic field lines.

In the case of sunspot-like structures the atmospheric cut-off lies around  $\sim 4$  mHz, so the modes with frequencies below this one will not be able to reach the high chromosphere. Many authors have argued before about the possibility of the non-linear interaction among 5-min modes being the source of the chromospheric 3-min oscillations (see, e.g. Fleck & Schmitz 1993). But if this were the case, the photospheric and chromospheric filtered velocity maps would show no resemblance with each other. As a matter of fact, a clear correlation exists, indicating that most of the 6 mHz power observed at chromospheric heights in sunspot-like structures comes directly from the same frequency range in the photosphere via upward linear wave propagation. This ratifies and extends the conclusions of Paper I (which focuses on the umbrae of big sunspots) to smaller sunspots and pores. As the size of the structure decreases, so does the typical radiative cooling time, while the temperature, on the other hand, grows. As argued before, both these behaviors are in agreement with what is expected from a qualitative point of view.

In the case of facular regions, the cut-off frequency stands around 2 mHz. This is accounted for in the model by introducing a shorter cooling time and a higher temperature. This allows the 5-min power to propagate through the atmosphere and reach the high chromosphere. Again, a clear correlation between photospheric and chromospheric filtered velocity maps can be found, indicating that the propagation is mainly linear and vertical within the 2–5 mHz range.

It is interesting to point out that, in this particular case, there is no need to invoke a large inclination of magnetic flux tubes to explain the p-mode leakage into the chromosphere (De Pontieu et al. 2004). Furthermore, the comparison of the photospheric and chromospheric velocity maps shows a good co-spatial correlation (after applying a convenient time shift) indicating that the propagation is essentially vertical. If we assume that the wave propagation takes place along the field lines and we take into account a height difference of 1000 - 1500 km, a magnetic field inclination of  $40 - 45^\circ$  would result in a spatial displacement of 3 - 5 pixels between the photospheric and the chromospheric oscillations (rather than happening on the same vertical). In the best case scenario, this displacement would be parallel to the slit; however, in the worst case, it would happen along the direction perpen-

dicular to the slit, leading to a correlation between the photosphere and the chromosphere that is marginally compatible with the spatial resolution of our data. On the other hand, the measured Stokes profiles set an upper limit of  $20^\circ$  on the inclination of the photospheric facular magnetic fields. Both these arguments point towards a magnetic field structure that is incompatible with the inclinations needed to lower the cut-off frequency enough to allow p-mode leakage.

The numerical simulations of Khomenko et al. (2008) have confirmed this conclusion since they show how, in a more realistic atmosphere, it is possible to explain the propagation of 5-minute modes into the chromosphere through vertical thin flux tubes, using radiative losses as the main ingredient to lower the cut-off frequency.

As the photospheric perturbations propagate upwards, their amplitude increases due to the rapid decrease in density and they eventually develop asymmetries that steepen more or less depending on the magnetic structure (the lower the magnetic flux, the smaller the amplification and the steepness of the developing shock). In all the cases, the time delay between photospheric and chromospheric oscillations is around several minutes in the frequency range near where the chromospheric power peaks.

This research was partially funded by the Spanish Ministerio de Educación y Ciencia through project AYA2007-63881. The National Center for Atmospheric Research (NCAR) is sponsored by the National Science Foundation

## REFERENCES

- Abdelatif, T.A, Thomas, J.H, 1987, ApJ, 320, 884
- Athay, G.R., White, O.R., 1979, ApJS, 39, 333.
- Avrett, E.H., Fontenla, J.M., Loeser, R., 1994, IAUS, 154, 35
- Ballesteros, E., Collados, M., Bonet, J. A., Lorenzo, F., Viera, T., Reyes, M. & Rodriguez Hidalgo, I., 1996, A&AS, 115, 353.
- Bard, S., Carlsson, M., 2008, ApJ, 682, 1376.
- Beckers, J.M., Tallant, P.E., 1969, Sol. Phys., 7, 351.
- Bogdan, T.J., Judge, P.G., 2006, Phil. Trans. R. Soc. London A, 364, 313.

- Brynildsen, N., Maltby, P., Fredvik, T., & Kjeldseth-Moe, O., 2004, in SOHO 13: Waves, Oscillations, and Small-Scale Transient Events in the Solar Atmosphere, ed. H. Lacoste (ESA SP-547; Noordwijk: ESA), 45
- Brynildsen, N., Maltby, P., & Kjeldseth-Moe, O. 2003, *A&A*, 398, L15
- Büntte, M., Bogdan, T.J., 1994, *A&A*, 283 642
- Centeno, R., Collados, M., Trujillo Bueno, J. 2006a, *ApJ*, 640, 1153.
- Centeno, R., Collados, M., Trujillo Bueno, J., 2006b, Proceedings of the Solar Polarization Workshop 4, ASP Conference Series, Vol. 358. Edited by R. Casini and B. W. Lites, p.465
- Centeno, R., Trujillo Bueno, J., Uitenbroek, H., Collados, M., 2008, *ApJ*, 677, 742.
- Centeno, R., Trujillo Bueno, J., Uitenbroek, H., Collados, M., to appear in the proceedings of the Solar Polarization Workshop 5.
- Collados, M. 1999, in ASP Conf. Ser. 184, Third Advances in Solar Physics Euroconference: Magnetic Fields and Oscillations, ed. B. Schmieder, A. Hofmann, & J. Staude (San Francisco: ASP), 3
- Collados, M., 2003, in "Polarimetry in Astronomy", edited by Silvano Fineschi, Proceedings of the SPIE, vol. 4843, pp. 55-65
- Collados, M., Trujillo Bueno, J., Bellot Rubio, L.R., Socas-Navarro, H., 2001, INTAS Workshop on MHD Waves in Astrophysical Plasmas, Universitat de les Illes Balears, pp. 151-154, Eds. J.L. Ballester and B. Roberts.
- De Pontieu, B., Erdelyi, R., De Moortel, I., 2005, *ApJ*, 624, 61.
- De Pontieu, B., Erdelyi, R., de Wijn, A.G., 2003, *ApJ*, 595, L63
- De Pontieu, B., Erdelyi, R., James, S.P, 2004, *Nature*, 430, 536
- Fleck, B. & Schmitz, F. 1993, *A&A*, 273, 671
- Gurman, J.B., Leichbacher, J.W., 1984, *ApJ*, 283, 859.
- Jefferies, S.M., McIntosh, S.W., Armstrong, J.D., Bogdan, T., Thomas, J., Cacciani, A. & Fleck, B. *ApJ*, 648, L151
- Khomenko, E., Centeno, R., Collados, M., Trujillo Bueno, J., 2008, *ApJ*, in press.

- Khomenko, E., Collados, M., 2006, *ApJ*, 653, 755.
- Kneer, F., Trujillo Bueno, J., 1987, *A&A*, 183, 91.
- Krijger, J.M., Rutten, R.J., Lites, B.W., Straus, T., Shine, R.A., Tarbell, T.D., 2001, *A&A*, 379, 1052.
- Lagg, A., 2007, *Advances in Space Research* 39, 1734.
- Leighton, R.B., Noyes, R.W., Simon, G.W., 1962, *ApJ*, 135, 474.
- Lites, B.W., 1986, *ApJ*, 301, 1005.
- Lites, B.W., 1986, *ApJ*, 301, 992.
- Lites, B. W. 1992, in *Sunspots: Theory and Observations*, ed. J. H. Thomas & N. O. Weiss, NATO ASI ser. C 375, Kluwer, Dordrecht, 261
- Lites, B.W., Rutten, R.J., Kalkofen, W., 1993, *ApJ*, 414, 354
- Martínez Pillet, V., Collados, M., Sánchez Almeida, J. et al., 1999, *High Resolution Solar Physics: Theory, Observations and Techniques*, ASP Conference Series 183, (eds.) T.R. Rimmele, K.S. Balasubramaniam, and R. Radick, 264.
- Mihalas, D., Wiebel-Mihalas, B., 1984, "Foundations of Radiation Hydrodynamics", Oxford University Press, Oxford.
- Roberts, B., 2006, *Royal Society of London Transactions Series A*, 364, Issue, 1839, 447.
- Ruiz Cobo, B., del Toro Iniesta, J.C., 1994, *A&A*, 283, 129.
- Sánchez-Andrade Nuño, B., Centeno, R., Puschmann, K.G., Trujillo Bueno, J., Blanco Rodríguez, J., Kneer, F., 2007, *A&A Letters*, in press.
- Sasso, C., Lagg, A., Solanki, S.K., 2005, *ESASP*, 596E, 64.
- Schmidt, W. & Kentischer, T., 1995, *A&AS*, 113, 363
- Schmidt, W., Knölker, M., Westendorp Plaza, C., 1994, *A&A*, 287, 229.
- Socas-Navarro, H., Trujillo Bueno, J., & Ruiz Cobo, B. 2000, *Science*, 288, 1396
- Souffrin, P., 1972, *A&A*, 17, 458.
- Spiegel, E.A., 1957, *ApJ*, 126, 202.

Thomas, J.H., 1983, AnRFM, 15, 321.

Trujillo Bueno, J., Asensio Ramos, A., 2007, ApJ, 655. 642.

White, O.R., Athay, G.R., 1979, ApJS, 39, 347.

Zhugzhda, Y.D., Locans, V., Staude, J., 1985, A&A, 143, 201.